Cancer Biol Med 2025. doi: 10.20892/j.issn.2095-3941.2024.0398

ORIGINAL ARTICLE

Nuclear PHGDH regulates macrophage polarization through transcriptional repression of *GLUD1* and *GLS2* in breast cancer

Pei Wang[1], Xin Du[1], Zhiren Han[1], Jiaxin Zhong[1], Jiayu Yuan[2], Lin Jiang[2], Beinan Han[1], Wenkui Fu[1], Hongde Li[3], Hai Hu[2,3,4], Zhenkun Na[3]*

[1]Department of Oncology, Sun Yat-sen Memorial Hospital, Sun Yat-sen University, Guangzhou 510120, China; [2]Postgraduate Training Base Alliance of Wenzhou Medical University, Zhejiang Cancer Hospital, Hangzhou 310022, China; [3]Hangzhou Institute of Medicine, Chinese Academy of Sciences, Zhejiang Cancer Hospital, Hangzhou 310018, China; [4]Breast Cancer Center, Zhejiang Cancer Hospital, Hangzhou Institute of Medicine, Chinese Academy of Sciences, Hangzhou 310022, China

ABSTRACT

Objective: Tumor-associated macrophages (TAMs) exhibit heterogeneous properties including anti-tumorigenic and pro-tumorigenic phenotypes. The rate-limiting enzyme in *de novo* serine biosynthesis, 3-phosphoglycerate dehydrogenase (PHGDH), has a well-established role in cellular metabolism, yet its specific role in macrophages remains unknown.

Methods: Metabolomics assays were conducted to assess metabolite composition and dynamics in macrophages. Changes in polarization and immunosuppressive markers were validated with qRT-PCR. Bioinformatics was used to analyze immune cell subsets and associated metabolic pathways. Finally, ChIP-qPCR and co-immunoprecipitation assays were performed to elucidate the downstream regulatory mechanisms of PHGDH.

Results: Serine metabolism was found to be downregulated in TAMs in breast cancer. Functional studies revealed that PHGDH inhibition promotes an M2-like phenotype and immunosuppressive functions in macrophages. Furthermore, PHGDH was found to undergo nuclear translocation during macrophage polarization. Mechanistically, nuclear PHGDH was found to regulate *GLUD1* and *GLS2* transcription *via* interaction with the transcription factor STAT3. Rescue experiments demonstrated that glutamine supplementation and STAT3 inhibition reversed the effects of PHGDH on macrophage function.

Conclusions: Our findings reveal a previously unrecognized non-canonical metabolic function of PHGDH, thus providing potential therapeutic targets in the tumor microenvironment for reversing malignant progression.

KEYWORDS Breast cancer; tumor-associated macrophages; serine metabolism; polarization

Introduction

Breast cancer is the most prevalent malignant tumor type and the leading cause of cancer-related mortality among women globally. This disease exhibits diverse biological characteristics in terms of pathology, genomics, gene expression, and the tumor microenvironment (TME)[1]. The optimization of therapy depends on the tumor subtype, anatomic cancer stage, and individual patient preferences[2]. Decreasing breast cancer mortality requires effectively addressing metastatic disease and overcoming resistance to systemic therapies[3].

The focus of recent research on metastasis and drug resistance has expanded from solely tumor cells to the inflammatory TME[4]. The intricate, multi-layered crosstalk between malignant and non-malignant cells in the TME is critical in breast cancer initiation and progression. The TME contributes to breast cancer heterogeneity and is instrumental in driving malignant progression[5]. Consequently, numerous strategies targeting the non-malignant cells and elements within the TME have been explored[6].

Among the various cellular components of the TME, tumor-associated macrophages (TAMs) are critical in mediating

*Lead contact.
Correspondence to: Hai Hu and Zhenkun Na
E-mail: huhai@zjcc.org.cn and nazhenkun@him.cas.cn
ORCID ID: https://orcid.org/0000-0001-6338-7431 and https://orcid.org/0009-0007-4197-5743
Received September 15, 2024; accepted November 14, 2024; published online May 28, 2025.
Available at www.cancerbiomed.org
©2025 The Authors. Creative Commons Attribution-NonCommercial 4.0 International License

the inflammatory process. TAMs are essential in tumor biology, by promoting tumor angiogenesis, metastasis, and immune evasion, and thereby driving tumor progression and contributing to therapeutic resistance[7]. Additionally, macrophages exhibit phenotypic heterogeneity and plasticity through a process known as polarization. In this dynamic process, macrophages react to stimuli from the surrounding microenvironment and adopt a distinct functional phenotype[8]. Macrophages are typically categorized into 2 functional states: the classically activated (M1) phenotype, which exhibits anti-tumorigenic properties, and the alternatively activated (M2) phenotype, which supports tumorigenesis[9]. Most TAMs in the TME have an M2-like phenotype. An emerging therapeutic strategy involves harnessing the plasticity of macrophages to reprogram them toward a tumoricidal phenotype. Reprogramming TAMs has been suggested to enhance the efficacy of immunotherapies by generating robust anti-tumor responses[10].

The TME's limited differentiated vascular system impairs nutrient and oxygen delivery, and requires immune cells to compete with rapidly proliferating cancer cells for essential resources[11]. These conditions induce metabolic adaptations in infiltrating immune cells that promote immune tolerance and suppress anti-tumor immunity. Targeting cellular metabolism offers promising therapeutic avenues in cancer treatment, particularly by modulating immune cell metabolism to enhance pro-inflammatory responses and optimize the efficacy of cancer therapies.

Immune cells establish distinct metabolic profiles in response to activation, adaptation to different tissue environments, inflammation, or disease[12]. In tumors, TAM reprogramming toward an anti-tumorigenic phenotype is tightly regulated at multiple levels, including transcriptional control and metabolic reprogramming[13]. Pro-tumorigenic TAMs, akin to alternatively activated (M2) macrophages, exhibit enhanced fatty acid uptake and glutamine metabolism, thus leading to elevated oxidative phosphorylation activity[14]. In contrast, anti-tumorigenic TAMs undergo metabolic shifts similar to those in classically activated (M1) macrophages, and are characterized by upregulated aerobic glycolysis, diminished oxidative metabolism, and tricarboxylic acid (TCA) cycle disruptions. These metabolic alterations underpin their anti-tumorigenic functions[15]. The divergent bioenergetic demands of M1 and M2 macrophages are increasingly recognized as critical regulatory mechanisms that influence macrophage behavior, thereby offering potential avenues for the development of future cancer therapies.

Serine can be obtained through both exogenous intake and *de novo* synthesis pathways[16], and phosphoglycerate dehydrogenase (PHGDH) is the initial rate-limiting enzyme in endogenous serine synthesis. PHGDH has been reported to have inconsistent effects on macrophage polarization; consequently, serine metabolism might have varying regulatory effects under different conditions. In this study, we applied metabolomics analysis methods in both benign and malignant inflammatory microenvironments, and found that glucose-serine-glycine-one-carbon metabolism differed significantly among TAMs. On the basis of these results, we further investigated the signaling pathway and molecular mechanisms associated with the above metabolic abnormalities in macrophages regulated in the microenvironment. Our results demonstrated that PHGDH undergoes nuclear translocation during polarization and regulates the transcription of *GLUD1* and *GLS2* by interacting with the transcription factor STAT3. In summary, our findings clarify abnormalities in key metabolic regulatory pathways that may serve as markers of disease progression and provide guidance regarding therapeutic strategies.

Materials and methods

Cells and cell culture

Six human cell lines were used: THP-1 [American Type Culture Collection (ATCC), Cat. TIB-202], HEK293T (ATCC, Cat. CRL-3216), MCF-7 (ATCC, Cat. HTB-22), MDA-MB-231 (ATCC, Cat. HTB-26), HCC1428 (ATCC, Cat. CRL-2327), and T-47D (ATCC, Cat. HTB-133). HEK293T, MCF-7, and MDA-MB-231 cells were cultured in DMEM (Gibco, Cat. 11965118) supplemented with 10% fetal bovine serum (Gibco, Cat. 10437028) and 1% penicillin–streptomycin (100 U/mL) (Gibco, Cat. 15140122). THP1, HCC1428, and T-47D were maintained in RPMI1640 (Gibco, Cat. 12633012) supplemented with 10% fetal bovine serum and 1% penicillin-streptomycin.

To initiate differentiation into M0 macrophage phenotype, we treated THP-1 cells with 100 ng/mL phorbol-12-myristate-13-acetate (PMA; MCE, Cat. HY-18739) for 24 h. M0 macrophages were then stimulated with 100 ng/mL lipopolysaccharide (MCE, Cat. HY-D1056) and 20 ng/mL IFN-γ (MCE, Cat. HY-P7025A) for 48 h to achieve M1 differentiation. For M2 polarization, M0 macrophages were stimulated with 20 ng/mL IL-4 (MCE, Cat. HY-P70445) and 20 ng/mL IL-13 (MCE, Cat. HY-P70568) for 48 h. For induction of TAMs, MDA-MB-231 cell conditioned medium (MB231-CM) was collected and

filtered. The MB231-CM was then combined in a 1:1 ratio with complete DMEM to create a medium suitable for TAM culture. M0 macrophages were then treated with MB231-CM for 48 h to generate TAMs. Correct differentiation into M1 and M2 type macrophages was confirmed through gene expression analysis of specific markers (such as IL1β, IL-6, TNF-α, IL-10, CD163, AGR1, TGF-β1, and CCL22).

Isolation and culture of mouse bone marrow-derived macrophages

C57BL/6 mice 6–8 weeks of age were euthanized and subsequently soaked in 75% ethanol. The skin from the lower part of the body was removed, and the tissue from the legs was carefully dissected. The bilateral femurs and tibias of the mice were isolated, and the muscles and tissues attached to the bones were removed. The bones were then immersed in 75% ethanol for 5 min and soaked in cold PBS for another 5 min. The cleaned bones were separated at the knee joint, and the ends of the leg bones were cut. Bone marrow cells were obtained by flushing of the femurs and tibias with cold induction medium. The cells were subsequently centrifuged at 1,500 rpm for 15 min and then resuspended with red cell lysate for approximately 2 min. DMEM was used to terminate the lysis process. After centrifugation at 300 g for 10 min, the cells were resuspended in DMEM containing 20% L929 conditioned medium. The medium was changed every 3 days, and bone marrow-derived macrophages (BMDMs) were induced to mature after 6–7 days. MB231-CM was then used to stimulate BMDMs for further analysis.

Stable cell line generation, and plasmid or small interfering RNA transfection

The PHGDH overexpression plasmid pcDNA3.1 and PHGDH small interfering RNA (siRNA) were synthesized by IGE Biotechnology, Guangzhou, China. BMDM cells were cultured in 6-well plates, and 3 μg plasmid or 50 nM siRNA was mixed with Advanced DNA Transfection Reagent (Zeta Life, USA, Cat. AD600150). The mixtures were added to 6-well plates after being incubated at room temperature for 15 min. After 48 or 72 h, transgene efficiency was assessed with quantitative real-time reverse transcriptase PCR (qRT-PCR) and Western blot analysis.

Lentiviral vectors were constructed by IGE Biotechnology, Guangzhou, China. The lentiviral vector and packaging plasmid were transfected into HEK293T cells to generate a viral suspension, which was subsequently used to transfect THP-1 cells. The viability of these cells was determined with Western blot and qRT-PCR.

Mouse studies

C57BL/6 mice were purchased from GemPharmatech and raised in the SPF animal facility at the Laboratory Animal Resource Center of Sun Yat-sen University. Female C57BL/6 mice 6–8 weeks of age were used. The mouse breast cancer cell line EO771 (ATCC, Cat. CRL-3461) was obtained from the ATCC and grown according to the standard protocols on the ATCC website. PHGDH overexpressing BMDMs (OE-PHGDH) and control BMDMs (OE-NC) were treated with IL-4/IL-13 for 24 h to induce polarization into immunosuppressive macrophages. Subsequently, they were cocultured with EO771 cells and injected into the fourth mammary fat pad on the right side in mice. EO771 cells (2×10^5) were mixed with 4×10^5 BMDMs in 100 μL PBS and used to induce the formation of subcutaneous tumors in mice. For macrophage ablation, mice received intraperitoneal injection of clodronate liposomes (150 μL/animal, twice per week) (Yeasen, Cat. 40337ES08). For tumor growth analysis, tumors were measured every 3 days with calipers, and tumor volume was calculated with the formula length × width × width/2. The mice were sacrificed 16 days after injection, and the tumors were removed for measurement and photography. The animal experimentation procedures received ethical approval under MSLT-2024-0121.

Immunohistochemistry staining

Mouse tissues were processed for formalin fixation, paraffin embedding, and tissue block sectioning. After deparaffinization and hydration, the sections were treated with H_2O_2 to block internal peroxidase activity. Citrate buffer (pH = 6) or Tris EDTA buffer (pH = 9) was subsequently used to retrieve antigens. Slides were blocked with goat serum for 30 min, then incubated overnight with rabbit anti-Ki-67 (Abcam, Cat. ab15580, 1:500) primary antibodies at 4°C. The next day, sections were incubated with goat anti-rabbit HRP (Abcam, Cat. ab205718, 1:2,000) for 1 h, then stained with hematoxylin and 3,3′-diaminobenzidine (Dako, Cat. ab64238) solutions. The images were captured under an OLYMPUS DP22 microscope, and ImageJ was used to assess the density of the immunohistochemistry staining.

Dual-luciferase reporter assays

The promoter sequences of *GLUD1* and *GLS2* in the pGL3-basic plasmid were synthesized by Generay Biotech, Shanghai, China. *GLUD1* in the pGL3-basic plasmid and *GLS2* in the pGL3-basic plasmid were transfected into TAMs induced by THP1 cells. The cells were treated as indicated in the figures and subsequently collected with passive lysis buffer. Luciferase activity was measured with a dual luciferase assay kit (Promega, Cat. E1910).

Analysis of immune infiltration in breast tumors

The infiltration of immune cells in the TME was quantified with the CIBERSORT analytical tool[17]. Gene expression data for 22 immune cell types were obtained from the CIBERSORT database. Subsequently, the data were uploaded to the CIBERSORT web platform and processed with the default signature matrix and enriched with 1,000 permutations to enhance the reliability of the results. With the CIBERSORT algorithm, a *P*-value was calculated for each deconvoluted sample with Monte Carlo sampling, thereby confirming the statistical significance and credibility of our results with high precision.

Correlation between serine metabolism and immune cell infiltration

The transcriptomic data and sample information for TCGA breast cancer data were obtained from the Xena database[18]. The CIBERSORT algorithm was used to assess immune cell infiltration. The correlations of *PHGDH*, *PSPH*, and *PSAT* expression with the infiltration levels of various immune cells were assessed with Pearson correlation analysis.

Metabolomics

THP1 cells were plated at a density of 3×10^6 cells per well in 6-well plates, washed, and harvested with 1 mL ice-cold 80% methanol. After being placed in a −80°C freezer for 30 min, the THP1 cells were transferred to a 2 mL tube. The dish was washed with 80% cold acetonitrile to ensure complete collection of cells. The samples were then rotary mixed at 4°C for 30 min and centrifuged at 12,000 rpm for 15 min at 4°C. The supernatant was collected and subsequently normalized by protein concentration for further analysis with BCA Protein Assay Kits (Thermo Fisher Scientific, Cat. 23225). The precipitate was kept at −80°C until mass spectrometry. For detection of intracellular metabolites, liquid chromatography-mass spectrometry was performed on an Agilent 1290 Infinity II UHPLC system (Santa Clara) at the Department of Oncology, Sun Yat-sen Memorial Hospital. The raw data were processed in MassHunter Workstation Software (version B.08.00, Agilent), and the peak areas of target compounds were integrated and output for quantitative calculation.

qRT-PCR

THP1 cells were plated at a density of 3×10^6 cells per well in a 6-well culture plate, then washed and harvested with an RNA extraction kit (Thermo Fisher Scientific, Cat. 12183020). Subsequently, cDNA was generated from 1 μg total RNA according to the manufacturer's instructions (Vazyme, Cat. R223-01). Real-time PCR was performed with qRT-PCR SYBR Master Mix (Vazyme, Cat. Q311-02).

Immunoblotting

THP1 cells were plated at a density of 3×10^6 cells per well in 6-well plates, lysed in RIPA buffer, and quantified with a BCA protein assay kit (Thermo Fisher Scientific, Cat. 23227). Subsequently, cell lysates (20 μg protein) were separated with SDS-PAGE and then transferred to polyvinylidene fluoride membranes (Millipore, Cat. IPVH00010). All membranes were blocked with 5% bovine serum albumin or nonfat milk in TBST buffer for 1 h, then incubated with the following primary antibodies: rabbit anti-PHGDH (Cell Signaling Technology, Cat. 66350, 1:1,000), rabbit anti-Arg1 (Cell Signaling Technology, Cat. 93668, 1:1,000), and rabbit anti-β-actin (Cell Signaling Technology, Cat. 4967, 1:1,000). After being washed with TBST buffer, the membrane was incubated with goat anti-rabbit IgG H&L (HRP) (ab6721, 1:5,000, Abcam, UK), then detected with enhanced chemiluminescence reagent (Thermo Fisher Scientific, Cat. 34580).

Nuclear and cytoplasmic protein was prepared with a Nuclear and Cytoplasmic Protein Extraction Kit (Beyotime, Cat. P0028) according to the manufacturer's instructions. Proteins from cell lysates were analyzed through Western

blot with the following antibodies: rabbit anti-PHGDH (Cell Signaling Technology, Cat. 66350, 1:1,000), rabbit anti-histone H3 (Cell Signaling Technology, Cat. 9715, 1:1,000), and rabbit anti-GAPDH (Cell Signaling Technology, Cat. 2118, 1:1,000).

Co-immunoprecipitation

Proteins were extracted from TAMs induced by THP1 cells (1×10^7) with IP lysis buffer (Thermo Fisher Scientific, Cat. 87787). Next, cell lysates were incubated with rabbit anti-PHGDH antibody (Cell Signaling Technology, Cat. 66350) at 4°C overnight. On the second day, the samples were mixed with Protein A/G agarose beads (Santa Cruz, Cat. sc-2003) for 2–3 h, then washed. The beads were boiled in 5× SDS-PAGE loading buffer (Fude, Cat. FD006) for 5 min and analyzed with Western blot. Mouse anti-STAT3 (Cell Signaling Technology, Cat. 9139, 1:1,000) and mouse anti-PHGDH (Abcam, Cat. ab57030, 1:1,000) served as the primary antibodies, whereas goat anti-Mouse IgG H&L (HRP) (Abcam ab6721, Cat. ab7063, 1:5,000) served as secondary antibodies for protein complex detection.

Chromatin immunoprecipitation (ChIP) and ChIP-qPCR

THP1 cells (1×10^7) were seeded in 100-mm dishes and treated with 1% formaldehyde (Sigma, USA, Cat. F8775) for crosslinking. Subsequently, 2.5 M glycine (Sigma, USA, Cat. G7126) was used to stop the crosslinking for 5 min at room temperature, and sonication was performed with a VirTis VirSonic 50 Ultrasonic Cell Disrupter at 4°C to shear chromatin into small fragments (150–300 bp). A 1% volume of the total sample was saved as input control. The anti-PHGDH antibody (Cell Signaling Technology, Cat. 66350) and rabbit IgG (Cell Signaling Technology, Cat. 2729) were added to the samples and rotary mixed at 4°C overnight. On the second day, chromatin immunoprecipitation (ChIP)-Grade Protein A/G Magnetic Beads (Thermo Fisher Scientific, Cat. 26162) were added to pull down the target protein, and elution buffer was used to resuspend the beads and isolate DNA.

Real-time PCR was performed to analyze the amount of bound DNA, and the enrichment value was calculated with the percentage input method. Primers covering the PHGDH binding site of the *GLUD1* or *GLS2* gene promoter region were used for qRT-PCR.

Immunofluorescence microscopy

Before immunofluorescence analysis, THP-1 cells (4×10^5) were treated with PMA for 24 h to induce differentiation into the M0 macrophage phenotype. After PMA treatment, the previously suspended THP-1 cells adhered to the culture surface. Subsequently, the cells were treated with MB231-CM for 48 h to induce TAMs. For immunofluorescence assays, M0 and TAMs were fixed with 4% paraformaldehyde on confocal dishes, then permeabilized with PBS containing 0.1% Triton X-100 (AR-0341, Dingguocs, Beijing, China) for 20 min. The cells were blocked with 5% bovine serum albumin in TBST buffer for 1 h at room temperature and then incubated with rabbit anti-PHGDH (1:500; Cell Signaling Technology, Cat. 32770) primary antibodies overnight at 4°C. On the second day, the cells were incubated with Alexa Fluor 488-labeled goat anti-rabbit IgG (1:200; Beyotime, Cat. A0423) secondary antibodies at room temperature for 1 h. Images were captured with a confocal microscope system (Zeiss LSM 780, Jena, Germany). Analysis was conducted in ImageJ.

Mouse single-cell RNA sequencing data analysis

For single-cell RNA sequencing (scRNA-seq) analysis, 6- to 8-week-old female BALB/c mice were used. The mouse breast cancer cell line 4T1 (ATCC, Cat. CRL-2359) was obtained from the ATCC and grown according to the standard protocols on the ATCC website. Approximately 1×10^6 4T1 cells in 100 μL PBS were injected into the fourth mammary fat pad in 6- to 8-week-old female BALB/c mice. The tumors were harvested for single-cell sequencing analysis after 4 weeks, to investigate the serine metabolic pathway in the TME.

For preparation of single-cell suspensions, mouse tumor tissue was dissected and minced with sterile scissors. The minced tissue was then transferred into a tube. Collagenase was used to digest the tissue at 37°C under shaking for 30 min. The cell suspension was subsequently filtered through a 40 μm mesh filter for single-cell sequencing analysis.

For alignment and expression matrix construction, raw FASTQ data were mapped to the GRCm39 reference genome (ENSEMBL release) with the 10× Genomics CellRanger pipeline (v8.0.0), and the expression count matrix was constructed *via* the cellranger count function with default settings.

For quality control, low-quality cells were removed according to the following criteria: (1) cells with > 300 detected genes; (2) cells with < 30% mitochondrial counts; and (3) cells with < 5% hemoglobin gene counts. Doublets were removed with the DoubletFinder pipeline, and genes expressed in fewer than 25 cells were excluded. A total of 19,338 genes and 14,051 cells passed quality control and were used in subsequent analysis.

For integration, dimensionality reduction, and cell annotation, the expression matrix was normalized and scaled with the Seurat pipeline, and sample integration was performed with Harmony. Dimensionality reduction was performed *via* the RunPCA function, and the top 30 PCs were used for UMAP analysis. A nearest-neighbor graph was generated, and cell clusters were defined with the Louvain algorithm at a resolution of 0.15. Cluster-specific marker genes were identified with Seurat's FindAllMarkers function, and clusters were annotated according to the biological relevance of their marker genes.

Statistical analysis

All continuous variables are represented as mean ± SD. Nonparametric variables were compared with the Chi-squared test. For parametric variables, a 2-tailed Student's *t*-test was used to indicate differences between 2 groups, or one-way analysis of variance was used for more than 2 groups. Kaplan–Meier analysis and log-rank test were used for survival analysis. $P < 0.05$ was considered statistically significant.

Results

M2 macrophages predict the prognosis of patients with breast cancer

Breast cancer is the most common malignancy in women and is classified as an inflammation-associated tumor[19,20]. To investigate the distribution of immune cells in breast cancer samples, we used the CIBERSORT algorithm on the TCGA BRCA database to quantify and compare the abundance of 22 distinct immune cell types. Macrophages emerged as the predominant immune cell subset in the TME (**Figure 1A**). Clinical evidence has established a significant correlation between TAMs and poor prognosis across various types of cancer[21]. We extended this analysis to breast cancer, for which survival analysis revealed that M1 macrophage infiltration had no substantial influence on overall survival outcomes. In contrast, lower infiltration of M2 macrophages was associated with a more favorable prognosis (**Figure 1B**). Additionally, the proportion of M2 macrophages progressively increased with advancing tumor stage, whereas no significant variation in M1 macrophage infiltration was observed across stages (**Figure 1C**). Together, these findings highlighted that macrophages are the predominant immune cell infiltrate, and M2 macrophage infiltration correlates with prognosis in patients with breast cancer.

Tumor-associated macrophages undergo metabolic reprogramming

Macrophages are highly plastic cells capable of altering their functional phenotype through polarization. In cancer, the TME actively reprograms macrophage metabolism, thereby regulating macrophage differentiation, polarization, mobilization, and the antitumor response. However, the metabolic alterations in TAMs are not fully understood.

To investigate the metabolic reprogramming in TAMs, we first differentiated THP-1 cells into M0 macrophages with PMA, then exposed them to conditioned medium from MDA-MB-231 tumor cell lines to mimic the TME *in vitro*. To confirm the induction effect, we incorporated proinflammatory (M1-like) and immunosuppressive (M2-like) macrophages as controls. The expression of proinflammatory cytokines, including *IL1β*, *IL-6*, and *TNF-α*, and immunosuppressive genes, such as *IL-10*, *CD163*, *AGR1*, *TGF-β1*, and *CCL22*, was measured. The expression of proinflammatory cytokines was comparable between M0 and TAMs. The transcriptional levels of immunosuppressive genes were greater in TAMs than M0 (**Figure 2A**). These results suggested that MDA-MB-231 conditioned medium promoted TAM polarization toward an M2-like phenotype. Subsequently, we used LC-MS/MS to profile the metabolic landscape of TAMs, and categorized the identified metabolites into 21 distinct chemical classes according to the Kyoto Encyclopedia of Genes and Genomes (KEGG). The numbers and percentage of metabolites in each chemical category are depicted in **Figure 2B**, thus illustrating the comprehensive coverage of pathway modules in this study. The glycolysis pathway was relatively more active in M1 macrophages (**Figure 2C**), whereas the tricarboxylic acid cycle was relatively more prominent in M2 macrophages (**Figure 2D**); in contrast, the metabolic pattern of TAMs was more consistent with M2 macrophages in the heatmap (**Figure 2E**). KEGG-based metabolic pathway

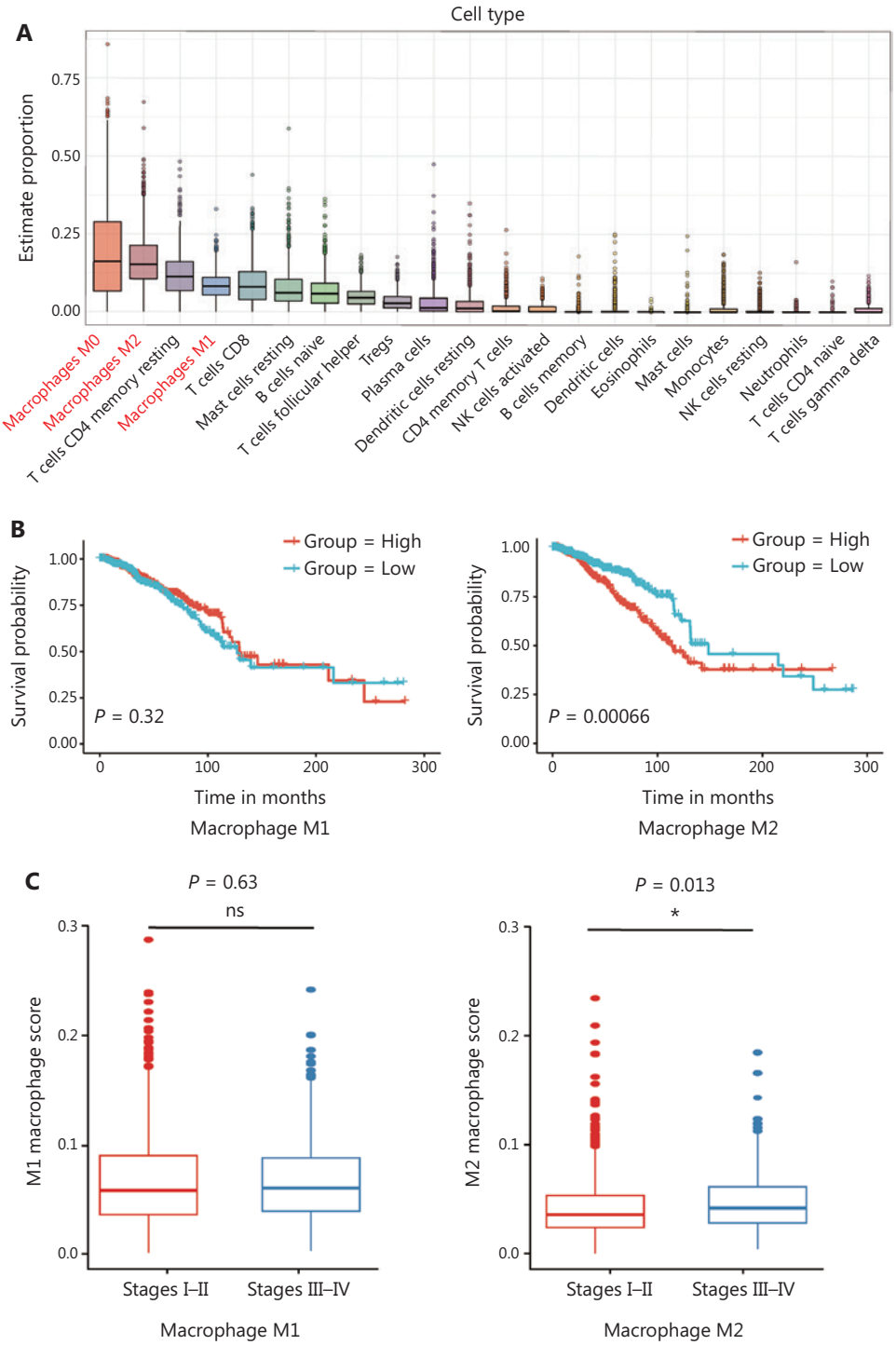


Figure 1 Effects of macrophages on breast cancer prognosis, according to tumor samples. (A) Immune cell subsets in primary breast cancer samples from CIBERSORT analysis of TCGA data (n = 1,097). The box plot illustrates the distribution of various immune cell infiltration levels. The immune cell types are systematically ordered from highest to lowest infiltration, according to the median infiltration proportion scores. (B) Kaplan–Meier curve comparing overall survival (OS) between patients with higher and lower M1 and M2 macrophage infiltration scores in the primary breast cancer samples from TCGA data. Log-rank P value is shown. (C) Immune infiltration analysis with the X cell algorithm conducted on a cohort of primary breast cancer samples from TCGA data with well-documented clinical stage information (n = 1,073). T-tests were used to compare the distribution differences in M1 and M2 macrophage infiltration scores between stages I and II (n = 805) and III and IV (n = 268) samples. *P < 0.05; ns: not significant.

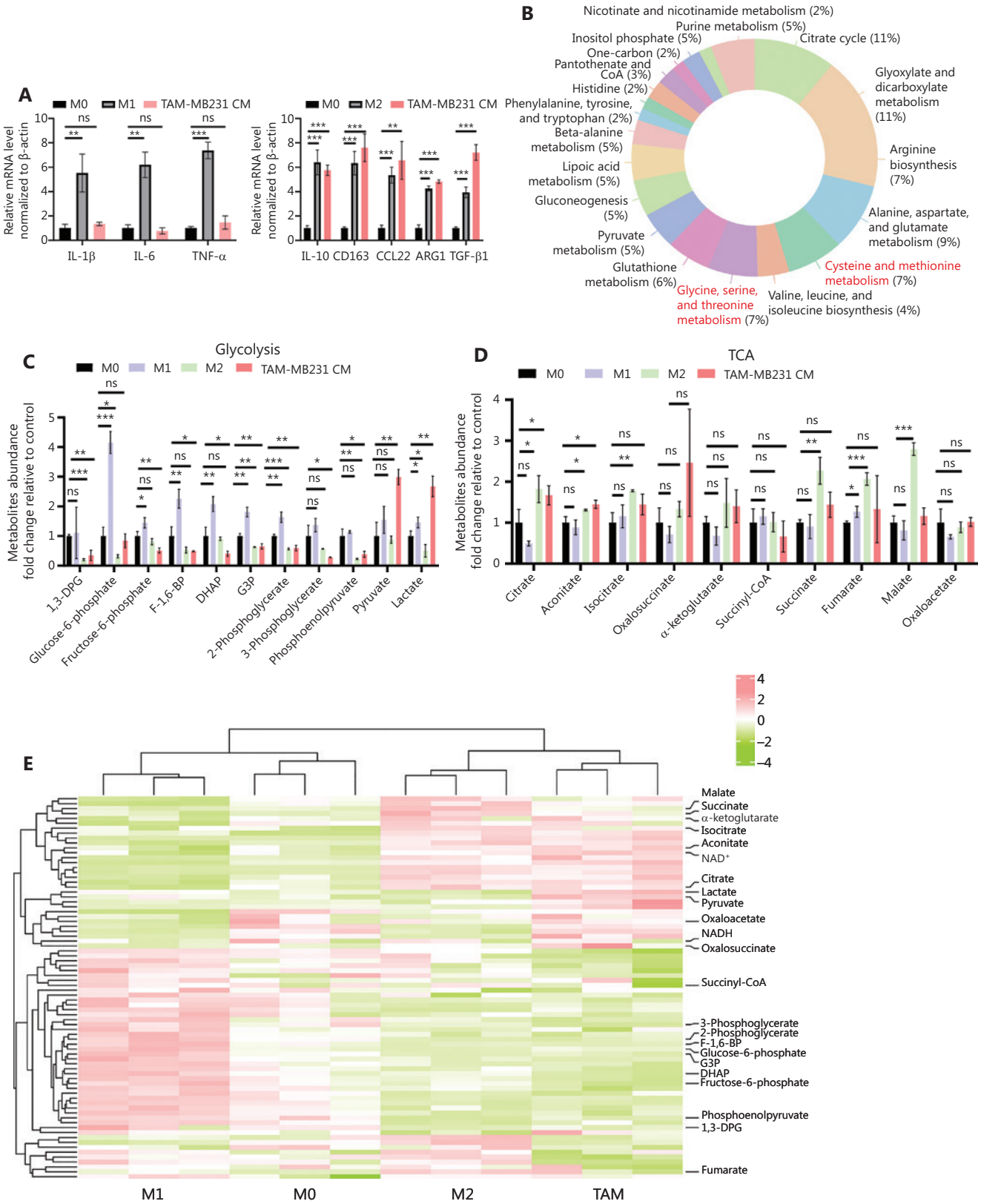


Figure 2 Continued

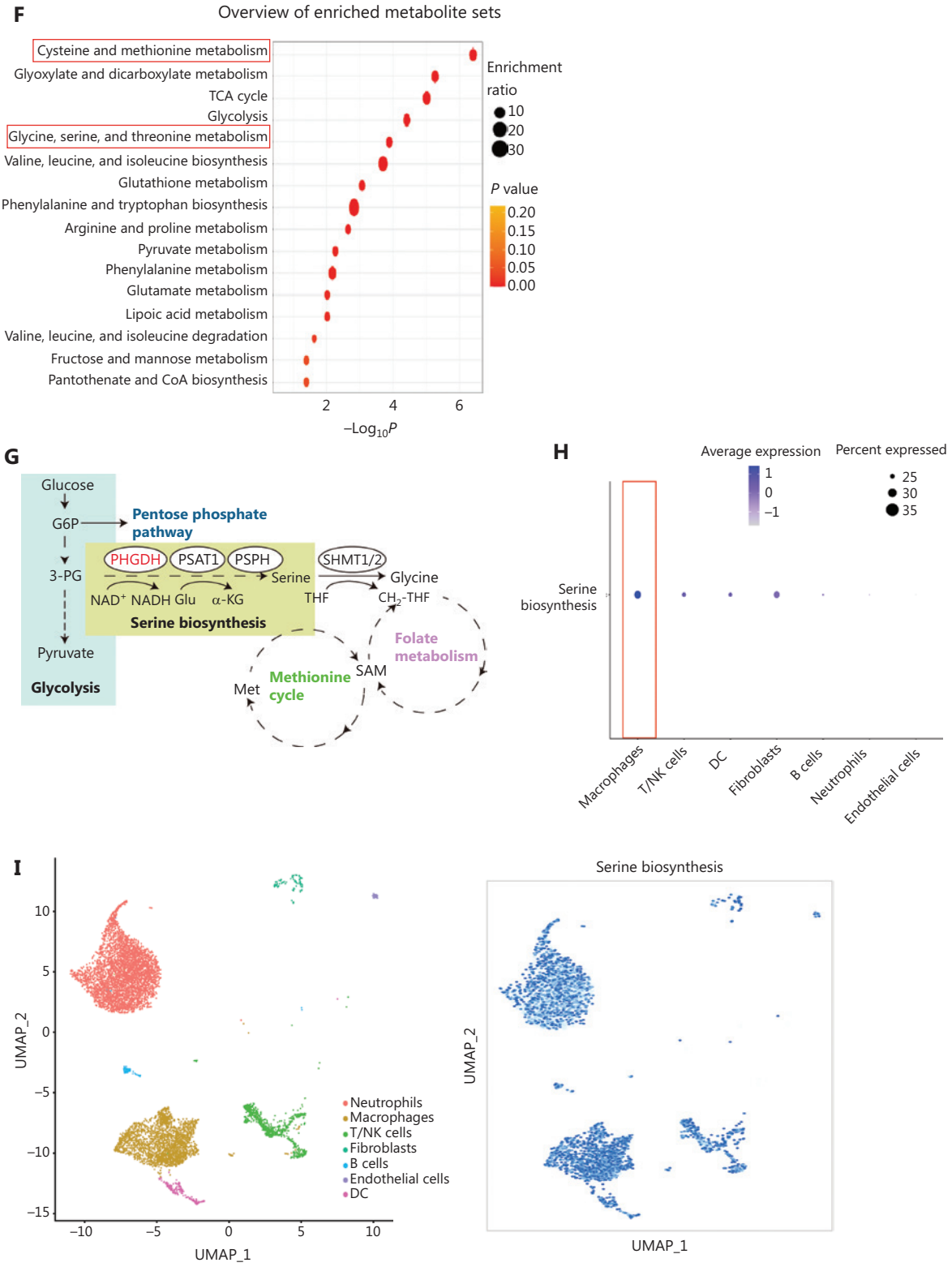


Figure 2 Metabolomic analysis of macrophages in breast cancer. (A) Differentiation of THP1 cells into macrophages for metabolomics analysis. THP-1 cells were differentiated after 24 h in PMA to obtain resting (M0) macrophages (n = 3). M0 macrophages were polarized toward M1 (n = 3) or M2 (n = 3) phenotypes through 48 h incubation with lipopolysaccharide and IFN-γ, or with IL-4 and IL-13. For obtaining

tumor-associated macrophages (n = 3), M0 macrophages were cultured in MDA-MB-231 cell conditioned medium (MB231-CM) for 48 h. Successful differentiation into tumor-associated macrophages was confirmed through gene expression analysis of specific markers (such as *IL1β*, *IL-6*, *TNF-α*, *IL-10*, *CD163*, *AGR1*, *TGF-β1*, and *CCL22*). M1 and M2 macrophages were incorporated as typing controls (**Table 1**). (B) Percentage of each metabolite class, detected by LC-MS/MS. (C) Levels of metabolites of glycolysis, determined *via* mass spectrometry (n = 3). (D) Levels of metabolites of the TCA cycle, determined *via* mass spectrometry. All metabolite levels were normalized to the control. Bar graphs represent the mean ± SD of experimental triplicates (t-test, $^*P < 0.05$, $^{**}P < 0.01$, $^{***}P < 0.001$). (E) Heatmap showing the distinct metabolic landscapes. (F) Metabolic pathway enrichment analysis of differential metabolites with MetaboAnalyst (https://www.metaboanalyst.ca) (t-test, $^*P < 0.05$, $^{**}P < 0.01$, $^{***}P < 0.001$). (G) Schematic of glycolysis and the PPP and the SSP metabolic pathways. (H) Bubble plot illustrating the expression levels of key enzymes in the serine biosynthesis pathway (PHGDH, PSAT1, and PSPH) across immune cell subgroups. Bubble size indicates the proportion of cells in a cell population expressing serine biosynthesis pathway proteins. Color represents the average expression of serine biosynthesis pathway components. (I) UMAP view of immune cell clusters from 2 samples (**Table 1**). UMAP plot depicting the serine biosynthesis pathway in immune cell clusters. $^*P < 0.05$, $^{**}P < 0.01$, $^{***}P < 0.001$, ns: not significant.

Table 1 Primers for validation

Genes	Forward primer	Reverse primer
β-actin	CTACCTCATGAAGATCCTCACCGA	TTCTCCTTAATGTCACGCACGATT
PHGDH	CTGCGGAAAGTGCTCATCAGT	TGGCAGAGCGAACAATAAGGC
PSAT1	TGCCGCACTCAGTGTTGTTAG	GCAATTCCCGCACAAGATTCT
PSPH	GAGGACGCGGTGTCAGAAAT	GGTTGCTCTGCTATGAGTCTCT
Shmt1	CTGGCACAACCCCTCAAAGA	AGGCAATCAGCTCCAATCCAA
Shmt2	CCCTTCTGCAACCTCACGAC	TGAGCTTATAGGGCATAGACTCG
TGF-β	GGCCAGATCCTGTCCAAGC	GTGGGTTTCCACCATTAGCAC
IL-10	GACTTTAAGGGTTACCTGGGTTG	TCACATGCGCCTTGATGTCTG
CD206	TCCGGGTGCTGTTCTCCTA	CCAGTCTGTTTTTGATGGCACT
CCL22	ATCGCCTACAGACTGCACTC	GACGGTAACGGACGTAATCAC
IDO	GCCAGCTTCGAGAAAGAGTTG	ATCCCAGAACTAGACGTGCAA
PD-L2	ATTGCAGCTTCACCAGATAGC	AAAGTTGCATTCCAGGGTCAC
PD-L1	GCTGCACTAATTGTCTATTGGGA	AATTCGCTTGTAGTCGGCACC
VISTA	ACGCCGTATTCCCTGTATGTC	TTGTAGAAGGTCACATCGTGC
LAG3	GCGGGGACTTCTCGCTATG	GGCTCTGAGAGATCCTGGGG
ASCT2	TCATGTGGTACGCCCCTGT	GCGGGCAAAGAGTAAACCCA
LAT1	CCGTGAACTGCTACAGCGT	CTTCCCGATCTGGACGAAGC
GLS	AGGGTCTGTTACCTAGCTTGG	ACGTTCGCAATCCTGTAGATTT
GLS2	GCCTGGGTGATTTGCTCTTTT	CCTTTAGTGCAGTGGTGAACTT
GOT2	AAGAGGGACACCAATAGCAAAAA	GCAGAACGTAAGGCTTTCCAT
GLUD1	GGGCTTTTGTATCCGTTACAGC	GGTCAAACGGCCATAGCTGA
GFAT	GGAATAGCTCATACCCGTTGG	TCGAAGTCATAGCCTTTGCTTT

enrichment analyses of differentially expressed metabolites with MetaboAnalyst 5.0 revealed that these metabolites were enriched primarily in cysteine and methionine metabolism pathways, and glycine, serine, and threonine metabolism pathways (**Figure 2F**). *De novo* serine synthesis branches off from glycolysis, and the glycolytic intermediate 3-phosphoglycerate

is directed into the serine synthesis pathway (SSP). Serine plays a crucial role in providing 1-carbon units to the folate cycle, thus supporting nucleotide synthesis and NADPH production[22]. Under certain circumstances, 1-carbon units can be integrated into the methionine cycle by recycling homocysteine to methionine (**Figure 2G**).

Simultaneously, we developed a preclinical model of triple-negative breast cancer by implanting 4T1 cells into BALB/c mice and subsequently conducted scRNA-seq. Notably, the key enzymes involved in the serine metabolic pathway (PHGDH, PSAT1, and PSPH) were significantly enriched in macrophages among the immune cells (**Figure 2H and 2I**).

The glycolysis branch pathways - the pentose phosphate pathway (PPP) and SSP and 1-carbon metabolism are down-regulated in tumor-associated macrophages

LC-MS/MS metabolomics analysis revealed a significant decrease in SSP metabolism after MB231-CM treatment (**Figure 3A**). A significant reduction in glycolytic flux was observed in TAMs, particularly affecting downstream pathways such as the PPP and one-carbon metabolism, was observed in TAMs (**Figure 3B and 3C**).

The restriction of exogenous serine or inhibition of the SSP influences macrophage polarization through various mechanisms[23-27]. These conflicting findings suggest that serine metabolism, including both exogenous uptake and *de novo* synthesis, exerts diverse regulatory effects on macrophage behavior under various conditions. Furthermore, previous studies have demonstrated that exogenous serine supplementation cannot compensate for the impairment in cell growth induced by PHGDH deletion[28], thus indicating that the function of the SSP extends beyond serine provision and may potentially include the activation of key transcription factors involved in polarization. We assessed the expression of key SSP enzymes at the gene level and observed that MB231-CM treatment downregulated these enzymes, as confirmed by qRT-PCR (**Figure 3D**).

Given the low expression of PHGDH in the MDA-MB-231 cell line, we hypothesized that crosstalk in serine metabolism might potentially exist between tumor cells and macrophages. THP1 cells were treated with conditional medium from 4 breast tumor cell lines, each with varying PHGDH expression. We observed an approximately 50% decrease in PHGDH mRNA expression in macrophages after stimulation with these media (**Figure 3E**), as further supported by Western blot findings (**Figure 3F**). Additionally, an increase in Arg1 protein levels confirmed the induction effect in TAMs (**Figure 3F**). These results suggested that PHGDH expression in tumor cells does not directly regulate serine metabolism in macrophages.

To further investigate the serine metabolic pathways in human samples, we conducted CIBERSORT immune infiltration analysis of primary breast cancer data, and observed a significant negative correlation between the expression of SSP metabolic enzymes and M2 macrophage infiltration levels (**Figure 3G**). Collectively, these findings indicated that serine metabolism is downregulated in TAMs in breast cancer.

PHGDH inhibition promotes the M2-like phenotype and immunosuppressive function in macrophages

To further elucidate the biological function of PHGDH in macrophages, we used a lentiviral vector system to achieve conditional expression of the PHGDH gene in THP-1 cells. The knockdown and overexpression of PHGDH were confirmed with qRT-PCR and Western blot (**Figure 4A and 4B**). Subsequently, we examined the influence of PHGDH on the expression of M2-like markers in TAMs treated with MB231-CM. Knockdown of PHGDH significantly upregulated the mRNA levels of M2-associated genes (*IL-10*, *CCL18*, *CCL22*, *TGF-β*, and *CD206*), as determined with qRT-PCR. In contrast, PHGDH overexpression markedly suppressed the expression of these M2 marker genes (**Figure 4E**). Furthermore, inhibition of PHGDH led to a significant increase in expression of the immune checkpoint genes *PD-L1* and *PD-L2* (**Figure 4G**).

Additionally, we investigated the function of PHGDH in mouse BMDMs. We transfected PHGDH specific siRNA (siPHGDH) and overexpression plasmid to regulate the expression of PHGDH (**Figure 4C and 4D**). Subsequently, we conducted the same experiment and obtained consistent results in BMDMs. Compared with the control group, the PHGDH overexpression group exhibited significantly downregulated expression of M2-associated genes (**Figure 4F**) and immune checkpoint genes (*PD-L1* and *PD-L2*) (**Figure 4H**). In contrast, the expression of M2 markers and immune checkpoint genes (*PD-L1* and *PD-L2*) in the siPHGDH group was significantly upregulated with respect to the control group. The consistent results in TAMs induced by THP1 and BMDM

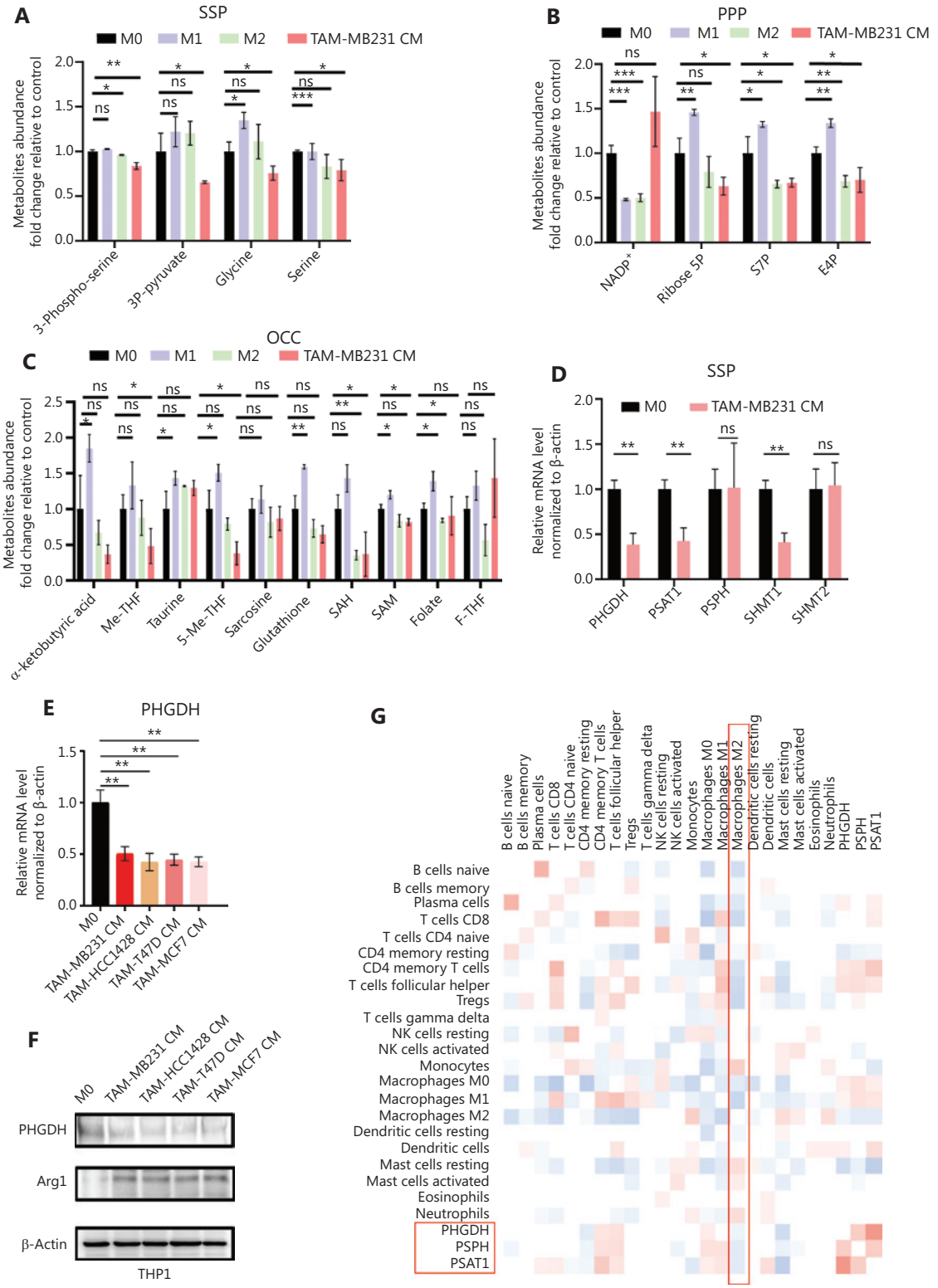


Figure 3 The serine metabolic pathway is downregulated in macrophages. (A) Levels of serine metabolic pathway metabolites in MDA-MB-231 cells after conditioned medium treatment. (B, C) Levels of metabolites of the PPP and 1-carbon metabolism, determined *via* mass spectrometry. All metabolite levels were normalized to the control. Bar graphs represent the mean ± SD of experimental triplicates (*t*-test, $^{*}P < 0.05$, $^{**}P < 0.01$, $^{***}P < 0.001$). (D) Relative mRNA expression of SSP metabolic pathways, assessed with qRT-PCR. (E, F) Relative mRNA expression

and protein expression levels of PHGDH in various macrophages. (G) CIBERSORT immune infiltration analysis of primary breast cancer tumor samples from TCGA (n = 1,097). The colors in each cell represent the correlation of the serine metabolic pathway with various immune cell infiltration levels. Red indicates positive correlation, blue indicates negative correlation, and white indicates a correlation coefficient of 0 or a correlation coefficient that is not statistically significant.

suggested that PHGDH inhibition promotes an M2-like phenotype and immunosuppressive function.

Additionally, we explored the relationship between *PHGDH* expression and macrophage-associated markers (*TGF-β* and *TNF-α*) in human breast cancer datasets (TCGA). We observed a significant negative correlation between *PHGDH* expression and the M2 macrophage marker *TGF-β* (R = −0.12, $P < 0.001$) and a positive correlation with the M1 macrophage marker *TNF-α* (R = 0.11, $P < 0.001$) in patients with breast cancer (**Figure 4I**). A weak correlation was found between *PHGDH* expression and other macrophage-associated markers (**Figure S1**).

To explore whether PHGDH might regulate macrophage polarization and consequently tumor growth *in vivo*, we transfected BMDMs (polarized by IL-4 and IL-13) with either a PHGDH-overexpressing plasmid or a control plasmid, and mixed them with EO771 cells. Subsequently, the mixed cells were injected into C57BL/6 mice (n = 7) (**Figure 4J**). Overexpression of PHGDH resulted in significantly lower tumor growth and tumor weight than observed in control tumors (**Figure 4K**). Consistently, fewer Ki67+ proliferating cells were found in tumors with PHGDH overexpression than in control tumors (**Figure 4L**). Collectively, these results suggested that PHGDH inhibition enhances M2-like macrophage polarization and immunosuppression function.

PHGDH knockdown induces metabolic changes in TAMs

To explore the effects of PHGDH on global metabolic remodeling, we performed LC-MS-based metabolomics analysis in TAMs treated with MB231-CM (**Figure 5A**). Beyond the observed decrease in serine-glycine-1-carbon pathway activity (**Figure 5C**), we identified significant metabolomic alterations in response to PHGDH suppression. Enrichment analysis of differentially expressed metabolites was performed with MetaboAnalyst 5.0. In PHGDH knockdown TAMs, we observed diminished activity of the glycolysis metabolism pathway, which is upstream of PHGDH (**Figure 5D**). Moreover, PHGDH knockdown led to a significant upregulation in arginine and glutamine levels (**Figure 5C**). Metabolites in the TCA cycle, compared with other metabolic pathways, were particularly affected by PHGDH knockdown (**Figure 5B**). Previous studies have established that pro-inflammatory macrophages depend primarily on glycolysis[29] and the PPP[14] for energy production, whereas M2 macrophages are more reliant on oxidative phosphorylation. Additionally, arginine and glutamine metabolism[30] have been shown to promote M2 polarization through multiple mechanisms. Collectively, these findings suggest that PHGDH knockdown induces metabolic reprogramming, and metabolic stress drives M2 polarization of macrophages.

The observation that PHGDH inhibition affected the TCA cycle prompted us to investigate the underlying mechanisms in greater detail. Notably, TCA cycle metabolites were elevated after the formation of the α-ketoglutarate (**Figure 5E**). In the mitochondria, glutamine is converted to glutamate, which subsequently serves as a precursor to α-ketoglutarate. Approximately one-third of the carbon atoms in the intermediates of the TCA cycle originate from glutamine (**Figure 5F**). Therefore, we hypothesized that PHGDH might influence macrophage polarization *via* glutamine metabolism. In addition, M2 macrophages preferentially use glutamine and fatty acids as energy sources, rather than glucose[12]. TAMs display elevated levels of glutamine transporters and metabolic enzymes[31]. Glutamine deprivation results in significant functional alterations in M2 macrophages.

PHGDH undergoes nuclear translocation, and negatively regulates GLUD1 and GLS2 after MB231-CM treatment

Next, we aimed to elucidate the function of PHGDH in glutamine metabolism. We analyzed the expression level of key metabolic enzymes involved in the conversion of glutamine to α-ketoglutarate through qRT-PCR and Western blot. Notably, PHGDH knockdown macrophages exhibited elevated

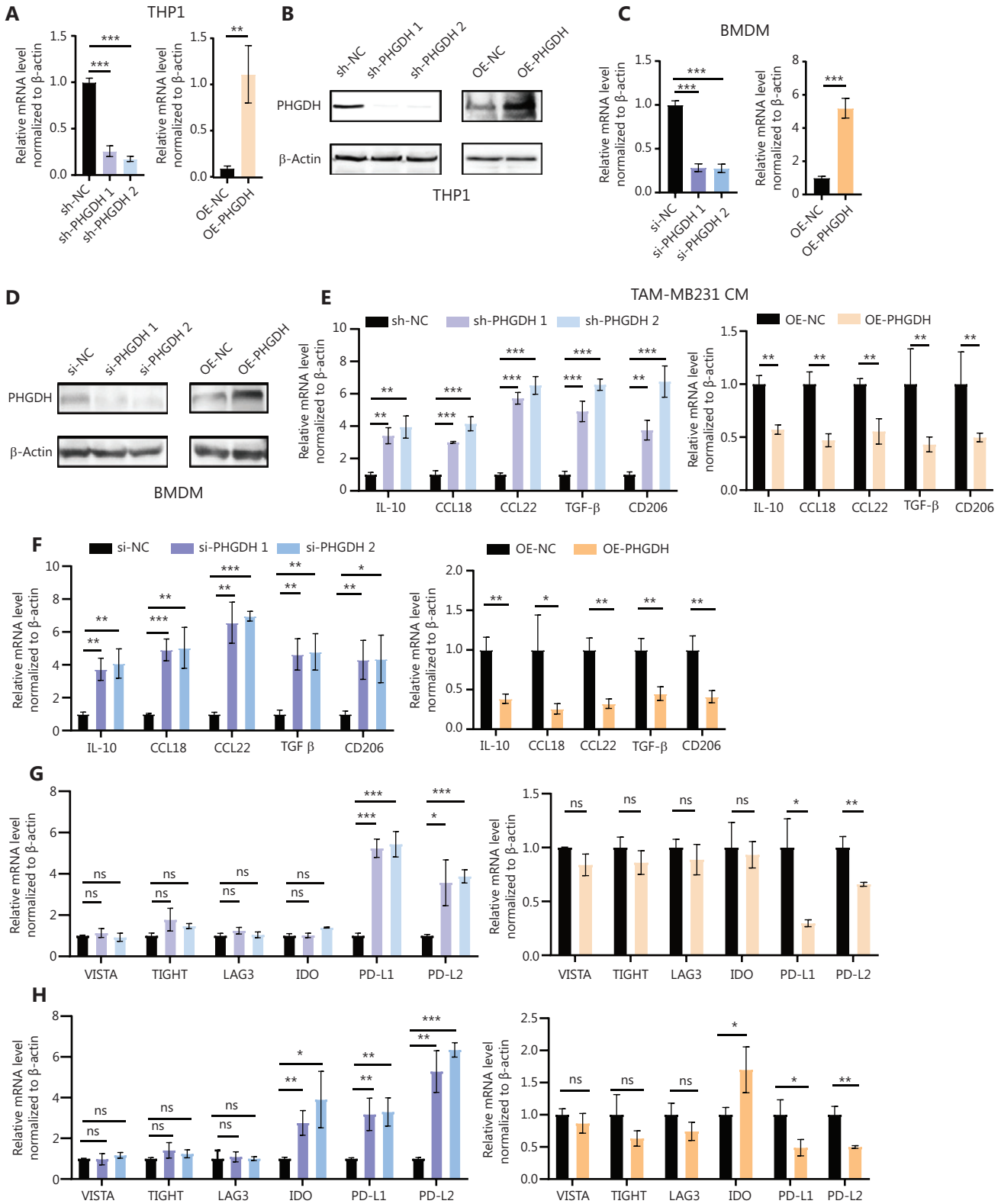


Figure 4 Continued

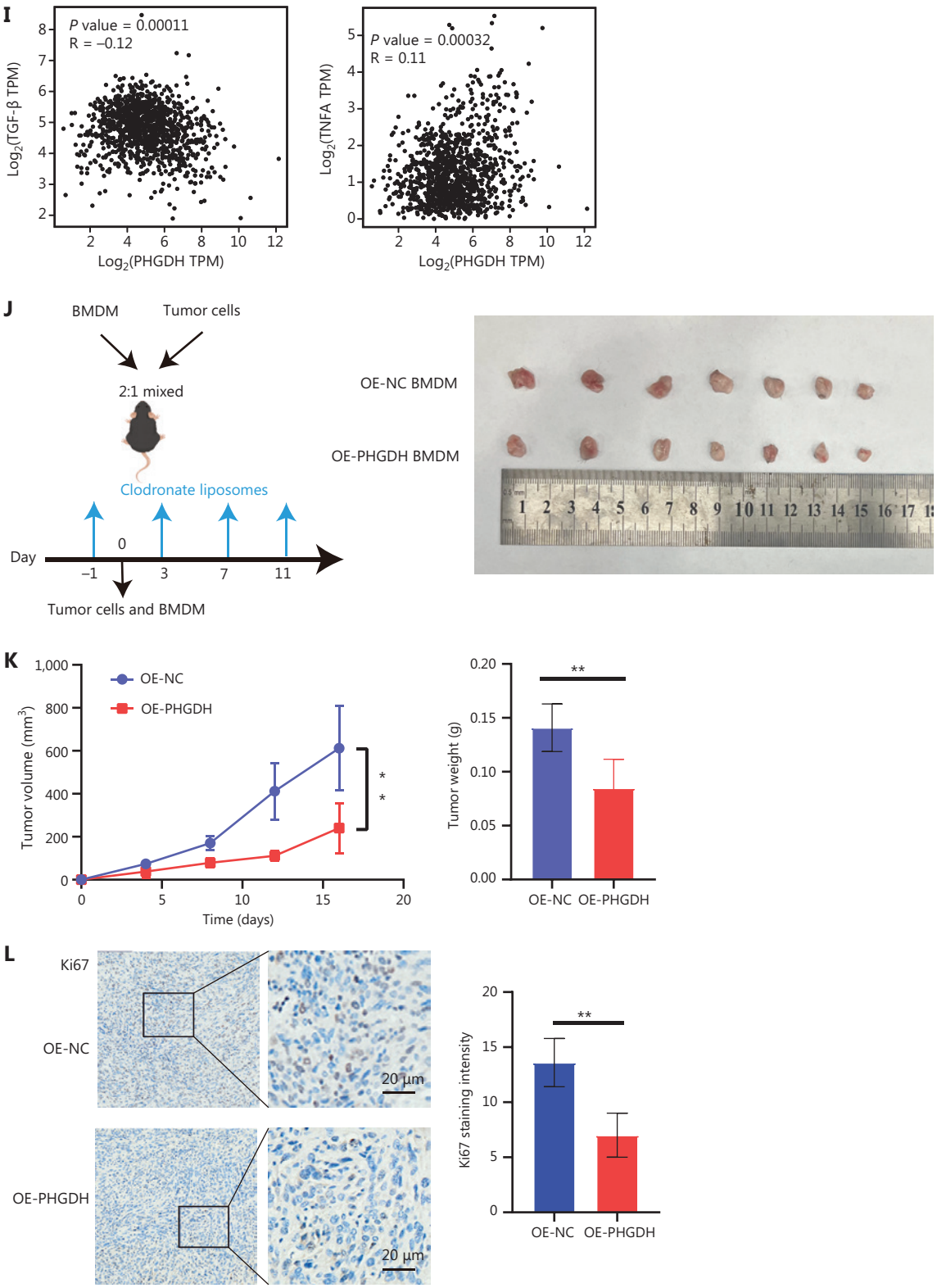


Figure 4 Inhibition of PHGDH enhances the M2-like macrophage polarization phenotype and immunosuppressive function. (A, B) Overexpression and knockdown of PHGDH validated at the mRNA level by qRT-PCR and the protein level by Western blot in THP1 cells. (C, D) Validation of overexpression and knockdown of PHGDH at the mRNA level by qRT-PCR and the protein level by Western blot in BMDM cells.

(E, F) Effects of PHGDH overexpression or knockdown in tumor-associated macrophages on polarization function and (G, H) immunosuppressive function (*t*-test, **P* < 0.05, ***P* < 0.01, ****P* < 0.001) (**Table 1**). (I) Correlation analyses of the transcriptional levels of macrophage-associated markers (*TGF-β* and *TNF-α*) with PHGDH in human breast cancer, according to data from the TCGA database. (J–L) PHGDH overexpressing BMDMs (OE-PHGDH) and control BMDMs (OE-NC) were mixed with EO771 cells and grafted into C57BL/6 mice (*n* = 7). (J) Schematic diagram of the cell transfer experiment and tumor image. (K) Growth curve and tumor weight (*t*-test, **P* < 0.05, ***P* < 0.01, ****P* < 0.001, *****P* < 0.0001, ns: not significant). (L) Representative immunohistochemistry images of paraffin-embedded xenograft sections. Scale bar, 20 μm.

expression of GLUD1 and GLS2 (**Figure 6A and 6B**), whereas macrophages with PHGDH overexpression showed significantly lower expression levels of these genes than observed in control cells (**Figure 6C and 6D**). Subsequently, we performed dual luciferase reporter assays to verify PHGDH's regulation of *GLUD1* and *GLS2* transcription. The transcription of *GLUD1* and *GLS2* was significantly enhanced by PHGDH loss-of-function (**Figure 6E**). ChIP-qPCR assays confirmed direct binding of PHGDH to the promoter regions of *GLUD1* or *GLS2* genes in macrophages (**Figure 6F**). These findings suggested that PHGDH suppresses the transcription of *GLUD1* and *GLS2*, thereby modulating glutamine-α-ketoglutarate metabolism in macrophages. Our results therefore revealed a previously unrecognized function of PHGDH in macrophages.

On the basis of our finding that manipulation of PHGDH regulated the expression of *GLUD1* and *GLS2*, we speculated that nuclear localization might be essential for PHGDH's transcriptional regulatory functions. As expected, the nuclear translocation of PHGDH was confirmed through confocal fluorescence microscopy during the polarization of M0 to TAMs (**Figure 6G**). This finding was further supported by consistent results from nuclear/cytosolic fragmentation (**Figure 6H**).

We further hypothesized that nuclear PHGDH might cooperate with specific transcription factors in regulating *GLUD1* and *GLS2* transcription. To identify these potential transcriptional partners, we conducted a sequential analysis of transcription factors implicated in *GLUD1* and *GLS2* regulation, then performed co-immunoprecipitation assays in TAMs to identify proteins binding PHGDH (**Figure 6I**). Nuclear PHGDH was found to mediate *GLUD1* and *GLS2* transcription through interactions with the transcription factor STAT3, as reported previously[32,33]. STAT3, a known key driver of macrophage polarization, integrates multiple signaling pathways[34,35]. Consequently, macrophages with nuclear PHGDH display a novel role in regulating glutamine metabolism independently of enzyme activity.

PHGDH inhibits macrophage function in a glutamine-dependent manner

Previous studies have established the critical role of glutamine in macrophage activation[13]. In agreement with those findings, glutamine deprivation resulted in down-regulation of immune and polarization markers (**Figure 7A**). Given the confirmed interaction between PHGDH and *GLUD1*/*GLS2*, we propose that PHGDH might drive metabolic reprogramming in macrophages *via* the modulation of glutamine catabolism. Up-regulation of GLS2 and GLUD1 controls α-ketoglutarate accumulation *via* glutaminolysis, thereby promoting M2 polarization *via* Jumonji domain-containing protein D3 (Jmjd3)-dependent demethylation at H3K27me3[30,36] (**Figure 7B**). Indeed, glutamine deprivation counteracted the effects of sh-PHGDH in enhancing macrophage polarization and immunosuppressive function (**Figure 7C**). Notably, glutamine deprivation did not affect the expression levels of *CCL22* in macrophages with PHGDH knockdown. These findings suggested that PHGDH inhibition enhances macrophage function by activating the glutamine catabolism pathway. Considering the verified interaction between PHGDH and STAT3, we further treated PHGDH knockdown cells with the STAT3 inhibitor W1131. qRT-PCR analysis demonstrated that W1131 effectively mitigated the effects of PHGDH knockdown on macrophage function (**Figure 7D**), thus suggesting that PHGDH drives metabolic reprogramming in macrophages through interaction with the transcription factor STAT3.

Discussion

Ongoing advancements in immunotherapy have markedly improved treatment outcomes for many patients with breast cancer in the past 2 decades. The rise of immune checkpoint inhibitors, antibody-drug conjugates, and cancer vaccines has driven an increase in immunotherapy-based clinical trials[37]. However, clinical observations have underscored that the TIME

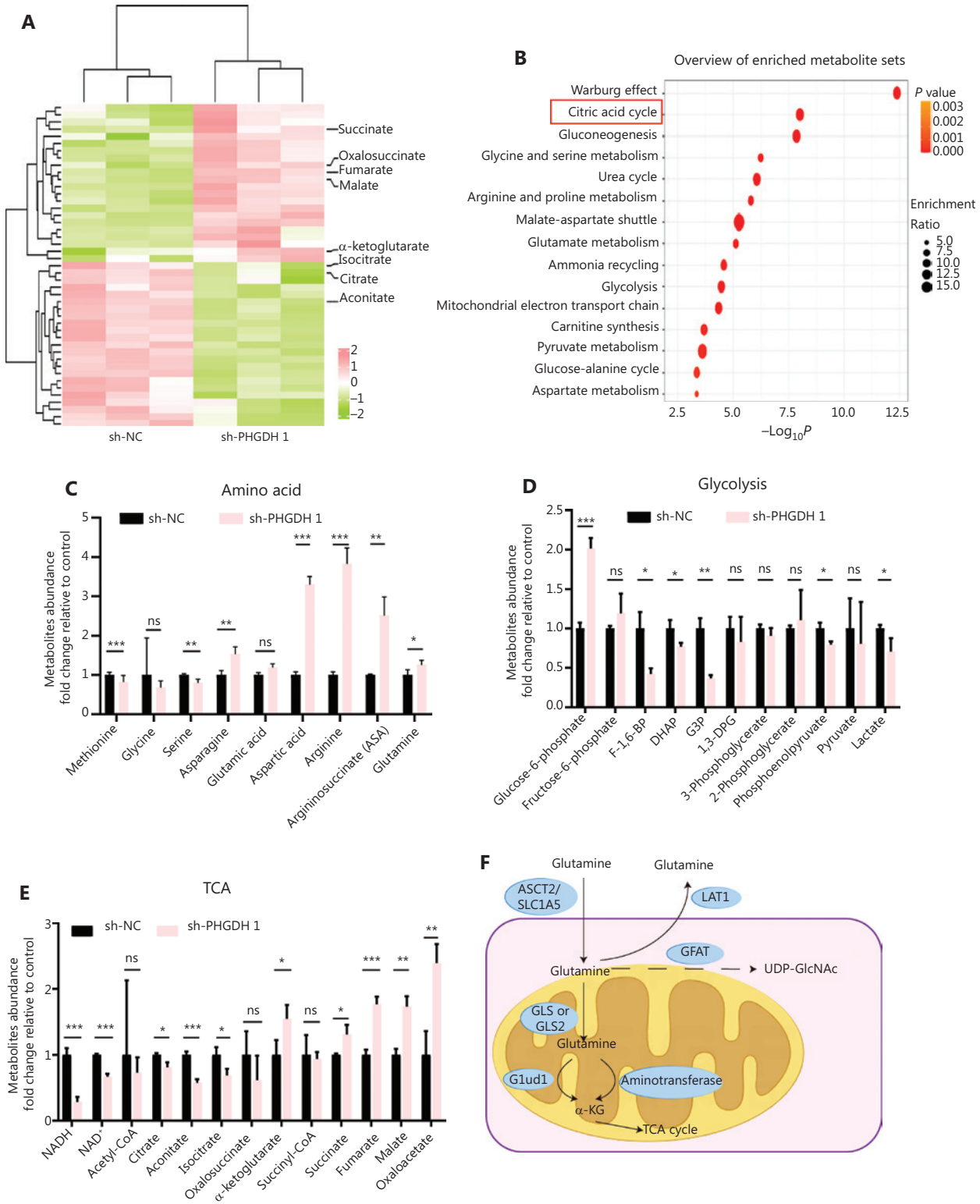


Figure 5 Intracellular metabolite profiling results of PHGDH knockdown. (A) Heatmap visualization of the distinct metabolic landscapes resulting from PHGDH knockdown. (B) Metabolic pathway enrichment of differential metabolites with MetaboAnalyst (https://www.metaboanalyst.ca). (C–E) Intracellular metabolites, assessed with mass spectrometry after cell transduction with sh-PHGDH. All metabolite levels are normalized to the control. Bar graphs represent the mean ± SD of experimental triplicates (*t*-test, **P* < 0.05, ***P* < 0.01, ****P* < 0.001). (F) Schematic of glutamine metabolism.

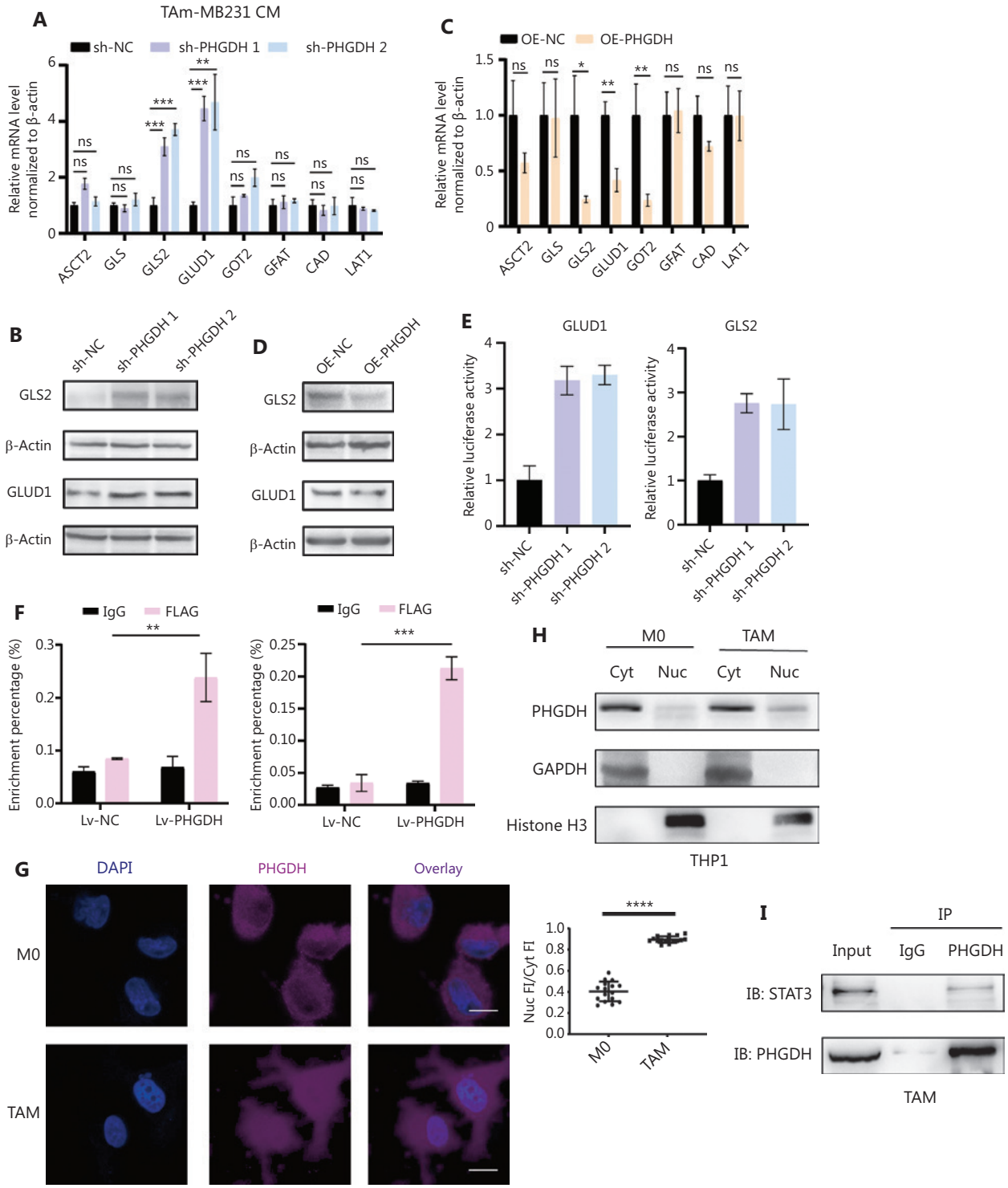


Figure 6 PHGDH cooperates with STAT3 in regulating *GLUD1* and *GLS2* transcription. (A, B) qRT-PCR and Western blot detection of changes in the glutamine metabolic pathway induced by PHGDH knockdown. (C, D) qRT-PCR and Western blot detection of changes in the glutamine metabolic pathway induced by PHGDH overexpression. (E) Dual-luciferase assay demonstrating that PHGDH knockdown increases the transcriptional activity of *GLUD1* and *GLS2* (**Table 2**). (F) ChIP and real-time PCR assays indicating PHGDH binding to the promoter region binding sites of *GLUD1* and *GLS2*. (G) Translocation of PHGDH in THP1 cells after treatment with MB231-CM, detected with confocal microscopy. Scale bar, 10 μm. (H) Translocation of PHGDH in THP1 cells after treatment with MB231-CM and nuclear/cytosolic fragmentation. (I) Co-immunoprecipitation of PHGDH in TAMs. Detection of PHGDH binding to STAT3 with Western blot (*t*-test, $^{*}P < 0.05$, $^{**}P < 0.01$, $^{***}P < 0.001$).

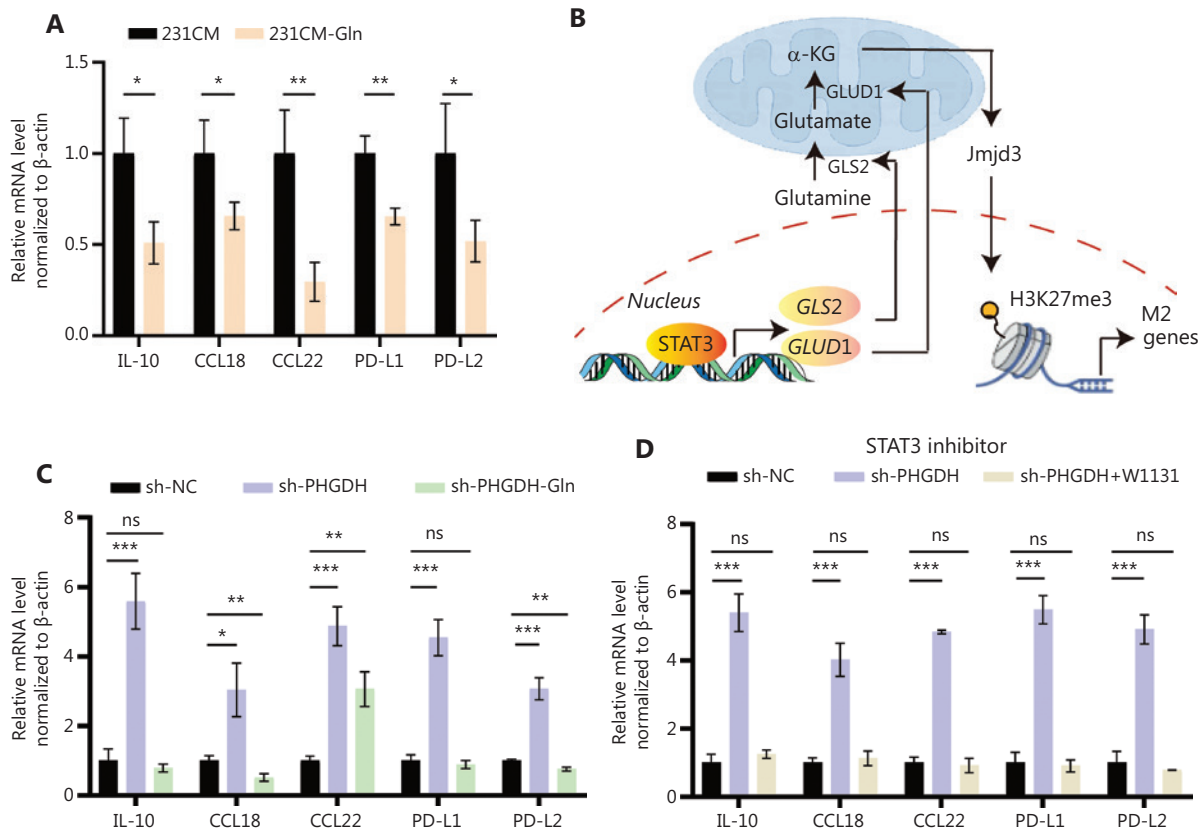


Figure 7 Inhibition of PHGDH promotes M2 macrophage polarization by activating the glutamine metabolic pathway. (A) Effects of glutamine deprivation on macrophage polarization and immunosuppressive function, determined with qRT-PCR. (B) Schematic overview of the molecular mechanism through which STAT3 regulates M2 genes. (C) Glutamine deprivation reversed the sh-PHGDH-mediated enhancement of macrophage polarization and immunosuppressive function. (D) Function of the STAT3 inhibitor W1131 (3 μM) on cytokine protein mRNA expression in PHGDH knockdown macrophages (**Table 1**). The results were obtained from three independent experiments. *P* values were calculated with one-way ANOVA. **P* < 0.05, ***P* < 0.01, ****P* < 0.001, ns: not significant.

Table 2 ChIP-qPCR primers used in the study

Genes	Forward primer	Reverse primer
GLUD1-ChIP-1	AGCTGCCAAACACCACATTAC	ACATATCGGGAAGCACCATCG
GLUD1-ChIP-2	CCTATGGATAGCTTTTGGTGCTTT	GTGGTGTTTGGCAGCTAGTTTTA
GLUD1-ChIP-3	GTGATGGTCGCGAAACAGGC	CTCCCCGTTAGGTGGCGAG
GLUD1-ChIP-4	CTCTCAGGTATGTGCGCCG	GACTCACATGACCCGGTCCC
GLUD1-ChIP-5	GGAGTTGGATTATGCGTGGC	CCACGACGTGCGTAACTATG
GLUD1-ChIP-6	GCTTTATGCTGTATGAGGGTTCAG	CGTTAGTTTGAAAAGCACCAAAAGC
GLS2-ChIP-1	GCCTTCTGCAGAGCCTTCAT	TTCTCCGTCTTCCAGGTCCA
GLS2-ChIP-2	AATGAGAGCAAGACGGTGGG	CTCAGCTTGTCCTCGCCTTT
GLS2-ChIP-3	GGCTGCGAATGATGGAGTTG	GGCTCTCTGAGTGACCTCCT
GLS2-ChIP-4	GGTGCTGAGTGGAGAGTAGG	GGGACACAAACTGGAACCCA
GLS2-ChIP-5	AAACCATGAAGTGCTCCCCA	CGCTGCCGAGATACAAGGTG
GLS2-ChIP-6	CCCATGGTGTTCCAACCGC	GCTGCATGAAGGAGAGACTTGTA

composition critically modulates the effectiveness of immunotherapy[38]. Given the critical roles of TAMs in modulating antitumor immunity, various therapeutic strategies targeting TAMs have been developed, including approaches for their repolarization, reprogramming, and depletion. Despite these efforts, the elimination of TAMs presents a substantial challenge, because it compromises macrophages' primary phagocytic and antigen-presenting function[39]. Therefore, reprogramming or repolarization of immunosuppressive TAMs into immunostimulatory phenotypes is a promising research avenue.

In this study, we conducted metabolomics analyses of both benign and malignant inflammatory microenvironments in breast cancer. Our findings demonstrated significant downregulation of the glucose-serine-glycine-1-carbon metabolism pathway in TAMs after treatment with conditioned media from 4 breast cancer cell lines with varying PHGDH expression. The results suggested that PHGDH expression in tumor cells does not directly regulate serine metabolism in macrophages, in agreement with prior findings[40]. Contrary to previous reports that PHGDH suppression promotes M1 macrophage polarization by increasing expression of IGF1 *via* S-adenosylmethionine, and that PHGDH contributes to the maintenance of an M2-like macrophage phenotype by activating mTORC1 signaling[26,27], our results demonstrated that PHGDH undergoes nuclear translocation during polarization. After translocation to the nucleus, PHGDH represses the M2-like macrophage polarization phenotype and immunosuppressive functions *via* glutamine metabolic pathways (**Figure 8**). Furthermore, our analysis of TCGA data revealed a negative correlation between the expression of metabolic enzymes in the SSP and the levels of M2 macrophage infiltration in primary tumor samples of breast cancer. Additionally, we observed a negative correlation between PHGDH expression and the M2 macrophage marker TGF-β in patients with breast cancer. This study provides a theoretical basis for reversing the malignant progression of tumors by targeting the metabolic pathways of immune inflammatory cells involved in malignant transformation.

Given the critical roles of both exogenous and endogenous serine synthesis in regulating cellular dynamics across cancer cells, lymphocytes, and endothelial cells[41], treatment with PHGDH inhibitors, and dietary restriction of serine and glycine, are being explored as promising anti-tumor therapies[42]. Recent studies have further implicated serine metabolism in macrophage polarization[43]. Previous research has demonstrated that serine supports M1 macrophage polarization through mechanisms involving mTOR signaling and the synthesis of S-adenosylmethionine and glutathione[23]. Furthermore, *de novo* serine synthesis has been found to mediate inflammatory responses by regulating IL-1β production through PHGDH-mediated NAD^+ accumulation[25]. However, some studies have reported that inhibiting PHGDH promotes M1 macrophage polarization; therefore, the roles of PHGDH and serine metabolism in TAMs remain unresolved. The contradictory effects of PHGDH on macrophage polarization might stem from variations in the disease models and tissue microenvironments. The increasing application of single-cell transcriptomics, epigenomics, metabolomics, and spatial multi-omics technologies has revealed the molecular and functional diversity of TAMs[44]. A comprehensive map of human macrophage diversity and development has identified 15 distinct macrophage subtypes[45]. Prior scRNA-seq studies have also challenged the view that alternative activation is the primary mechanism driving TAM heterogeneity[46]. Further research is required to elucidate the function of PHGDH in different macrophage subsets.

In recent years, extensive evidence has emerged indicating that the functional regulation of metabolic enzymes extends beyond their canonical roles in specific pathways and includes non-canonical or non-metabolic activities. These enzymes can be spatially and temporally regulated, and consequently act as regulatory molecules by modulating the activities of transcription factors[47]. The inability of exogenous serine supplementation to rescue the cell growth impairment caused by PHGDH depletion suggests that the function of PHGDH extends beyond serine production. A previous study has reported that PHGDH undergoes nuclear translocation after phosphorylation by p38 under glucose deficiency conditions. Nuclear PHGDH exerts a repressive effect on nuclear NAD^+ levels, owing to its enhanced catalytic activity for malate oxidation and NADH generation *via* AMPK activation[28]. In this study, we demonstrated that PHGDH undergoes nuclear translocation during M0 macrophage polarization to TAMs, and inhibits TAM function in a glutamine-dependent manner. Specifically, nuclear PHGDH represses the transcription of *GLUD1* and *GLS2* transcription through direct interaction with the transcription factor STAT3 (**Figure 8**), which acts as a critical regulator of macrophage plasticity by integrating multiple signaling pathways[34].

Several limitations of this study should be acknowledged. First, our research focused primarily on cellular level investigations. However, to comprehensively elucidate the complexity of human cancer biology, further studies at the clinical level

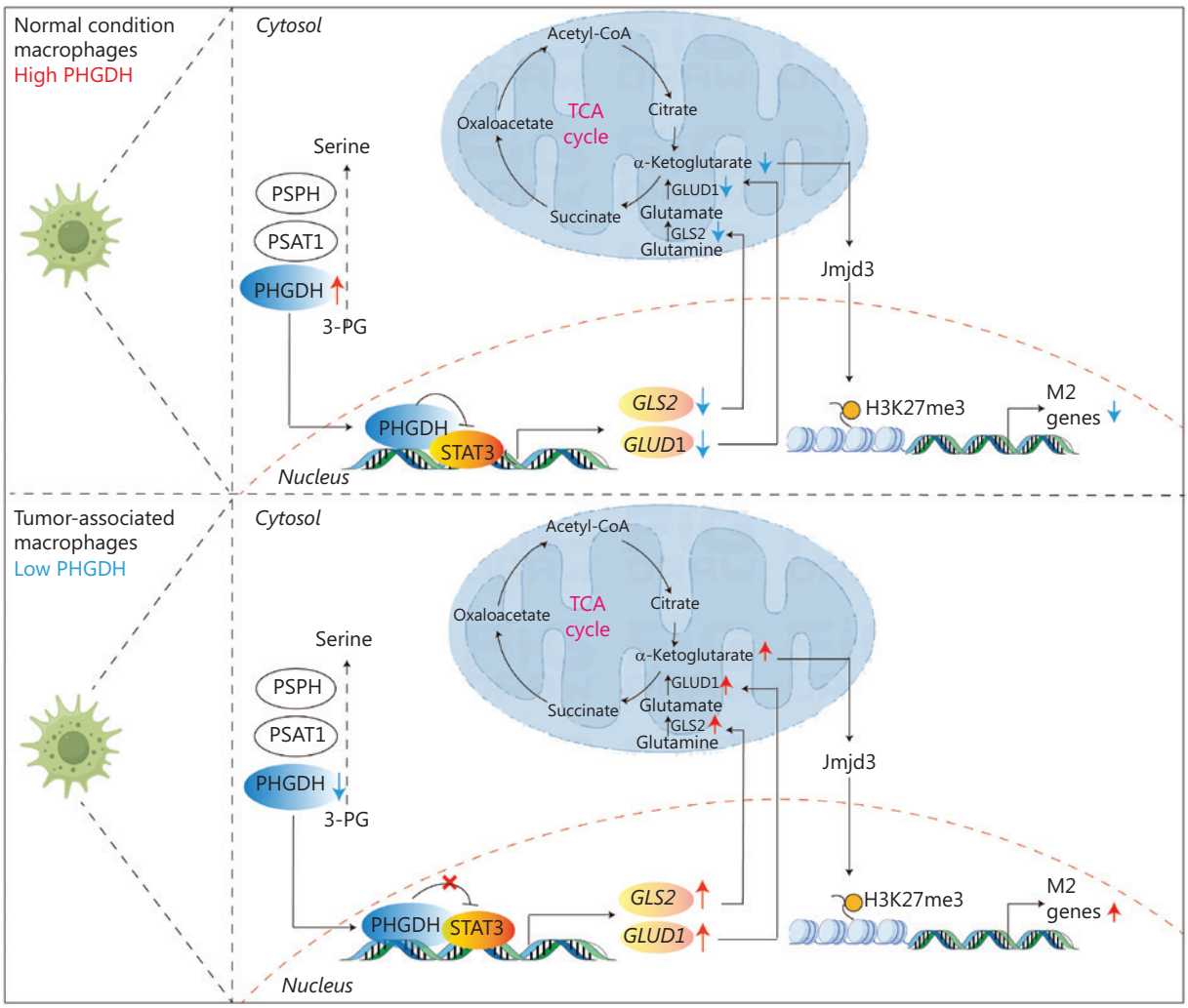


Figure 8 Schematic overview of the molecular mechanism through which PHGDH regulates macrophage function. During the polarization of M0 macrophages into TAMs, PHGDH, the initial rate-limiting enzyme in endogenous serine synthesis, translocates to the nucleus. PHGDH exhibits low expression in TAMs but high expression under normal conditions. In the nucleus, PHGDH interacts with the transcription factor STAT3, thereby suppressing transcription of the key metabolic regulators GLUD1 and GLS2. The downregulation of GLUD1 and GLS2 decreases glutaminolysis and α-ketoglutarate (α-KG) synthesis, thereby inhibiting Jmjd3-dependent epigenetic reprogramming of M2 genes[30,36].

will be essential. Additionally, further research is needed to identify the specific nutrient conditions that facilitate PHGDH nuclear translocation and to determine the molecular modifications required for this process.

Conclusions

In summary, our study elucidated the mechanism through which PHGDH regulates macrophage function and consequently reshapes the anti-tumor response. These findings highlight PHGDH as a potential diagnostic and therapeutic target for breast cancer and may provide a critical theoretical foundation for the development of novel therapies targeting inflammatory cells in the TME.

Grant support

This work was supported by grants from the National Key R&D Program of China (Grant No. 2022YFC3401001), National Natural Science Foundation of China (Grant Nos. 82025026 and 82230091 to H.H.), Key R&D Program of Zhejiang (Grant No. 2024C03160), and GuangDong Basic and Applied Basic Research Foundation (Grant Nos. 2023A1515012412 and 2023A1515011214).

Conflict of interest statement

No potential conflicts of interest are disclosed.

Author contributions

Conceived and designed the analysis: Pei Wang, Hai Hu, Zhenkun Na, Xin Du, Hongde Li.
Collected the data: Pei Wang, Jiaxin Zhong, Beinan Han.
Contributed data or analysis tools: Pei Wang, Jiayu Yuan, Lin Jiang, Wenkui Fu.
Performed the analysis: Pei Wang, Xin Du, Zhiren Han.
Wrote the paper: Pei Wang.

Data availability statement

The data generated in this study are available upon request from the corresponding author.

References

1. Herschkowitz JI, Simin K, Weigman VJ, Mikaelian I, Usary J, Hu Z, et al. Identification of conserved gene expression features between murine mammary carcinoma models and human breast tumors. Genome Biol. 2007; 8: 1-17.
2. Gennari A, André F, Barrios CH, Cortés J, de Azambuja E, DeMichele A, et al. ESMO Clinical Practice Guideline for the diagnosis, staging and treatment of patients with metastatic breast cancer. Ann Oncol. 2021; 32: 1475-95.
3. Torre LA, Bray F, Siegel RL, Ferlay J, Lortet-Tieulent J, Jemal A. Global cancer statistics, 2012. CA Cancer Journal Clin. 2015; 65: 87-108.
4. Qian BZ, Pollard JW. Macrophage diversity enhances tumor progression and metastasis. Cell. 2010; 141: 39-51.
5. Mehraj U, Dar AH, Wani NA, Mir MA. Tumor microenvironment promotes breast cancer chemoresistance. Cancer Chemother Pharmacol. 2021; 87: 147-58.
6. Belli C, Trapani D, Viale G, D'Amico P, Duso BA, Della Vigna P, et al. Targeting the microenvironment in solid tumors. Cancer Treat Rev. 2018; 65: 22-32.
7. Goswami KK, Ghosh T, Ghosh S, Sarkar M, Bose A, Baral R. Tumor promoting role of anti-tumor macrophages in tumor microenvironment. Cell Immunol. 2017; 316: 1-10.
8. Lopez-Yrigoyen M, Yang CT, Fidanza A, Cassetta L, Taylor AH, McCahill A, et al. Genetic programming of macrophages generates an in vitro model for the human erythroid island niche. Nat Commun. 2019; 10: 881.
9. Yunna C, Mengru H, Lei W, Weidong C. Macrophage M1/M2 polarization. Eur J Pharmacol. 2020; 877: 173090.
10. Guerriero JL, Sotayo A, Ponichtera HE, Castrillon JA, Pourzia AL, Schad S, et al. Class IIa HDAC inhibition reduces breast tumours and metastases through anti-tumour macrophages. Nature. 2017; 543: 428-32.
11. DeBerardinis RJ, Chandel NS. Fundamentals of cancer metabolism. Sci Adv. 2016; 2: e1600200.
12. Andrejeva G, Rathmell JC. Similarities and distinctions of cancer and immune metabolism in inflammation and tumors. Cell Metab. 2017; 26: 49-70.
13. Kowal J, Kornete M, Joyce JA. Re-education of macrophages as a therapeutic strategy in cancer. Immunotherapy. 2019; 11: 677-89.
14. Jha AK, Huang SC, Sergushichev A, Lampropoulou V, Ivanova Y, Loginicheva E, et al. Network integration of parallel metabolic and transcriptional data reveals metabolic modules that regulate macrophage polarization. Immunity. 2015; 42: 419-30.
15. O'Neill L AJ, Pearce EJ. Immunometabolism governs dendritic cell and macrophage function. J Exp Med. 2016; 213: 15-23.
16. Labuschagne CF, Van Den Broek NJF, Mackay GM, Vousden KH, Maddocks OD. Serine, but not glycine, supports one-carbon metabolism and proliferation of cancer cells. Cell Rep. 2014; 7: 1248-58.
17. Newman AM, Liu CL, Green MR, Gentles AJ, Feng W, Xu Y, et al. Robust enumeration of cell subsets from tissue expression profiles. Nat Methods. 2015; 12: 453-7.
18. Goldman MJ, Craft B, Hastie M, Repecka K, McDade F, Kamath A, et al. Visualizing and interpreting cancer genomics data via the Xena platform. Nat Biotechnol. 2020; 38: 675-8.
19. Nie Y, Chen J, Huang D, Yao Y, Chen J, Ding L, et al. Tumor-associated macrophages promote malignant progression of breast phyllodes tumors by inducing myofibroblast differentiation. Cancer Res. 2017; 77: 3605-18.
20. Gierach GL, Lacey JV Jr, Schatzkin A, Leitzmann MF, Richesson D, Hollenbeck AR, et al. Nonsteroidal anti-inflammatory drugs and breast cancer risk in the National Institutes of Health–AARP Diet and Health Study. Breast Cancer Res. 2008; 10: 1-13.
21. Condeelis J, Pollard JW. Macrophages: obligate partners for tumor cell migration, invasion, and metastasis. Cell 2006; 124: 263-6.
22. Fan J, Ye J, Kamphorst JJ, Shlomi T, Thompson CB, Rabinowitz JD. Quantitative flux analysis reveals folate-dependent NADPH production. Nature 2014; 510: 298-302.
23. Chen S, Xia Y, He F, Fu J, Xin Z, Deng B, et al. Serine supports IL-1β production in macrophages through mTOR signaling. Front Immunol. 2020; 11: 1866.
24. Rodriguez AE, Ducker GS, Billingham LK, Martinez CA, Mainolfi N, Suri V, et al. Serine metabolism supports macrophage IL-1β production. Cell Metab. 2019; 29: 1003-11.e4.
25. Wang C, Chen Q, Chen S, Fan L, Gan Z, Zhao M, et al. Serine synthesis sustains macrophage IL-1β production via NAD^+-dependent protein acetylation. Mol Cell. 2024; 84: 744-59.e6.
26. Shan X, Hu P, Ni L, Shen L, Zhang Y, Ji Z, et al. Serine metabolism orchestrates macrophage polarization by regulating the IGF1–p38 axis. Cell Mol Immunol. 2022; 19: 1263-78.

27. Cai Z, Li W, Hager S, Wilson JL, Afjehi-Sadat L, Heiss EH, et al. Targeting PHGDH reverses the immunosuppressive phenotype of tumor-associated macrophages through α-ketoglutarate and mTORC1 signaling. Cell Mol Immunol. 2024; 21: 448-65.
28. Ma C, Zheng K, Jiang K, Zhao Q, Sha N, Wang W, et al. The alternative activity of nuclear PHGDH contributes to tumour growth under nutrient stress. Nat Metab. 2021; 3: 1357-71.
29. Freemerman AJ, Johnson AR, Sacks GN, Milner JJ, Kirk EL, Troester MA, et al. Metabolic reprogramming of macrophages: glucose transporter 1 (GLUT1)-mediated glucose metabolism drives a proinflammatory phenotype. J Biol Chem. 2014; 289: 7884-96.
30. Liu PS, Wang H, Li X, Chao T, Teav T, Christen S, et al. α-ketoglutarate orchestrates macrophage activation through metabolic and epigenetic reprogramming. Nat Immunol. 2017; 18: 985-94.
31. Palmieri EM, Menga A, Martín-Pérez R, Quinto A, Riera-Domingo C, De Tullio G, et al. Pharmacologic or genetic targeting of glutamine synthetase skews macrophages toward an M1-like phenotype and inhibits tumor metastasis. Cell Rep. 2017; 20: 1654-66.
32. Mojzeš A, Tomljanović M, Milković L, Kujundžic RN, Gašparovic AC, Trošelj KG. Cell-type specific metabolic response of cancer cells to curcumin. Int J Mol Sci. 2020; 21: 1661.
33. He X, Tan S, Shao Z, Wang X Latitudinal and longitudinal regulation of tissue macrophages in inflammatory diseases. Genes & Diseases, 2022; 9: 1194-207.
34. Xia T, Zhang M, Lei W, Yang R, Fu S, Fan Z, et al. Advances in the role of STAT3 in macrophage polarization. Front Immunol. 2023; 14: 1160719.
35. Zhang G, Lu J, Zheng J, Mei S, Li H, Zhang X, et al. Spi1 regulates the microglial/macrophage inflammatory response via the PI3K/AKT/mTOR signaling pathway after intracerebral hemorrhage. Neural Regen Res. 2023; 19: 161-70.
36. Zhou W, Hu G, He J, Wang T, Zuo Y, Cao Y, et al. SENP1-Sirt3 signaling promotes α-ketoglutarate production during M2 macrophage polarization. Cell Rep. 2022; 39: 110660.
37. Debien V, De Caluwé A, Wang X, Piccart-Gebhart M, Tuohy VK, Romano E, et al. Immunotherapy in breast cancer: an overview of current strategies and perspectives. NPJ Breast Cancer 2023; 9: 7.
38. Binnewies M, Roberts EW, Kersten K, Chan V, Fearon DF, Merad M, et al. Understanding the tumor immune microenvironment (TIME) for effective therapy. Nat Med. 2018; 24: 541-50.
39. Wang YC, Wang X, Yu J, Ma F, Li Z, Zhou Y, et al. Targeting monoamine oxidase A-regulated tumor-associated macrophage polarization for cancer immunotherapy. Nat Commun. 2021; 12: 3530.
40. Hu X, Ma Z, Xu B, Li S, Yao Z, Liang B, et al. Glutamine metabolic microenvironment drives M2 macrophage polarization to mediate trastuzumab resistance in HER2-positive gastric cancer. Cancer Commun. 2023; 43: 909-37.
41. Kurniawan H, Franchina DG, Guerra L, Bonetti L, -Baguet LS, Grusdat M, et al. Glutathione restricts serine metabolism to preserve regulatory T cell function. Cell Metab. 2020; 31: 920-36.
42. Maddocks OD, Berkers CR, Mason SM, Zheng L, Blyth K, Gottlieb E, et al. Serine starvation induces stress and p53-dependent metabolic remodelling in cancer cells. Nature. 2013; 493: 542.
43. Wilson JL, Nägele T, Linke M, Demel F, Fritsch SD, Mayr HK, et al. Inverse data-driven modeling and multiomics analysis reveals Phgdh as a metabolic checkpoint of macrophage polarization and proliferation. Cell Rep. 2020; 30: 1542-52.
44. Pathria P, Louis TL, Varner JA. Targeting tumor-associated macrophages in cancer. Trends Immunol. 2019; 40: 310-27.
45. Wang Z, Wu Z, Wang H, Feng R, Wang G, Li M, et al. An immune cell atlas reveals the dynamics of human macrophage specification during prenatal development. Cell. 2023; 186: 4454-71.
46. Azizi E, Carr AJ, Plitas G, Cornish AE, Konopacki C, Prabhakaran S, et al. Single-cell map of diverse immune phenotypes in the breast tumor microenvironment. Cell. 2018; 174: 1293-308.
47. Boon R, Silveira GG, Mostoslavsky R. Nuclear metabolism and the regulation of the epigenome. Nat Metab. 2020; 2: 1190-203.

Cite this article as: Wang P, Du X, Han Z, Zhong J, Yuan J, Jiang L, et al. Nuclear PHGDH regulates macrophage pola6rization through transcriptional repression of *GLUD1* and *GLS2* in breast cancer. Cancer Biol Med. 2025; 22: 502-524. doi: 10.20892/j.issn.2095-3941.2024.0398